Translational development of ABCB5+ dermal mesenchymal stem cells for therapeutic induction of angiogenesis in non-healing diabetic foot ulcers

Mark Andreas Kluth (Andreas.kluth@ticeba.com)
TICEBA GmbH, Heidelberg https://orcid.org/0000-0003-0764-4645

Andreas Kerstan
Department of Dermatology, Venereology and Allergology, University Hospital Würzburg

Kathrin Dieter
RHEACELL GmbH & Co. KG, Heidelberg

Elke Niebergall-Roth
TICEBA GmbH, Heidelberg

Sabrina Klingele
TICEBA GmbH, Heidelberg

Michael Jünger
Department of Dermatology, University Hospital Greifswald

Christoph Hasslacher
Clinical Study Center St. Josefskrankenhaus, Heidelberg

Georg Daeschlein
Clinic of Dermatology, Immunology and Allergology, Medical University Brandenburg "Theodor Fontane" Medical Center Dessau

Lutz Stemler
Diabetologikum DDG Ludwigshafen

Ulrich Meyer-Pannwitt
pro scientia med at the Department of Clinical Research and Development, MARE Clinic, Kiel

Kristin Schubert
medamed GmbH, Leipzig

Gerhard Klausmann
Studienzentrum Aschaffenburg

Titus Raab
Diabetologikum Raab, Kassel

Matthias Goebeler
Department of Dermatology, Venereology and Allergology, University Hospital Würzburg

Korinna Kraft
RHEACELL GmbH & Co. KG, Heidelberg

Jasmina Esterlechner
TICEBA GmbH & Co. KG, Heidelberg
Hannes M. Schröder
RHEACELL GmbH & Co. KG, Heidelberg
Samar Sadeghi
TICEBA GmbH, Heidelberg
Seda Ballikaya
TICEBA GmbH, Heidelberg
Martin Gasser
Department of Surgery, University Hospital Würzburg
Ana M. Waaga-Gasser
Division of Renal (Kidney) Medicine, Brigham and Women's Hospital, Harvard Medical School, Boston
George F. Murphy
Brigham and Women's Hospital Department of Dermatology
Dennis P. Orgill
Division of Plastic Surgery, Brigham and Women's Hospital, Harvard Medical School, Boston
Natasha Y. Frank
Department of Medicine, VA Boston Healthcare System
Christoph Ganss
TICEBA GmbH, Heidelberg
Karin Scharffetter-Kochanek
Department of Dermatology and Allergic Diseases, University Hospital Ulm
Markus H. Frank
Brigham and Women's Hospital Department of Dermatology

Research Article

Keywords: ABCB5, Advanced-therapy medicinal product, Angiogenesis, Chronic wound, Diabetic foot ulcer, Mesenchymal stem cells, Wound healing

Posted Date: April 5th, 2022

DOI: https://doi.org/10.21203/rs.3.rs-1508134/v1

Abstract

Background

While rapid healing of diabetic foot ulcers (DFUs) is highly desirable to avoid infections, amputations and life-threatening complications, DFUs often respond poorly to standard treatment. GMP-manufactured skin-derived ABCB5$^+$ mesenchymal stem cells (MSCs) might provide a new adjunctive DFU treatment, based on their remarkable skin wound homing and engraftment potential, their ability to adaptively respond to inflammatory signals, and their wound healing-promoting efficacy in mouse wound models and human chronic venous ulcers.

Methods

The angiogenic potential of ABCB5$^+$ MSCs was characterized with respect to angiogenic factor expression at the mRNA and protein level, *in-vitro* endothelial trans-differentiation and tube formation potential, and perfusion-restoring capacity in a mouse hindlimb ischemia model. Finally, the efficacy and safety of ABCB5$^+$ MSCs for topical adjunctive treatment of chronic, standard therapy-refractory, neuropathic plantar DFUs was assessed in an open-label single-arm clinical trial.

Results

Hypoxic incubation of ABCB5$^+$ MSCs led to posttranslational stabilization of the hypoxia-inducible transcription factor 1α (HIF-1α) and upregulation of HIF-1α mRNA levels. HIF-1α pathway activation was accompanied by upregulation of vascular endothelial growth factor (VEGF) transcription and increase in VEGF protein secretion. Upon culture in growth factor-supplemented medium, ABCB5$^+$ MSCs expressed the endothelial-lineage marker CD31, and after seeding on gel matrix, ABCB5$^+$ MSCs demonstrated formation of capillary-like structures comparable with human umbilical vein endothelial cells. Intramuscularly injected ABCB5$^+$ MSCs to mice with surgically induced hindlimb ischemia accelerated perfusion recovery as measured by laser doppler blood perfusion imaging and enhanced capillary proliferation and vascularization in the ischemic muscles. Adjunctive topical application of ABCB5$^+$ MSCs onto therapy-refractory DFUs elicited median wound surface area reductions from baseline of 59% (full analysis set, n = 23), 64% (per-protocol set, n = 20) and 67% (subgroup of responders, n = 17) at week 12, while no treatment-related adverse events were observed.

Conclusions

The present observations identify GMP-manufactured ABCB5$^+$ dermal MSCs as a potential, safe candidate for adjunctive therapy of otherwise incurable DFUs and justify the conduct of a larger, randomized controlled trial to validate the clinical efficacy.

Trial registration: ClinicalTrials.gov, NCT03267784, Registered 30 August 2017, https://clinicaltrials.gov/ct2/show/NCT03267784

Background

Diabetic foot ulcers (DFUs) are among the most common and potentially serious complications of diabetes mellitus, with an estimated 19% to 34% of diabetes patients developing a DFU during their lifetimes [1]. Around 40% of patients who have developed a DFU die within 5 years [2-4]. While a significant proportion of the mortality rates can be attributed to fatal cardio-vascular complications of diabetes [5-7], the ulcer contributes independently to mortality due to inflammatory sequelae [4, 8, 9]. Specifically, more than half of DFUs become infected [10], with roughly 20% to 50% of moderate-to-severe diabetic foot infections potentially leading to some grade of lower extremity amputation [1, 11-14]. Many patients who underwent a DFU-related amputation have a poor quality of life and a high risk of premature death [15].

While rapid healing is highly desirable to avoid infections, amputations and life-threatening complications [16-18], DFUs often respond poorly to standard treatment. Reported healing failure rates range from roughly 40% to 80% at 12 weeks and still from 15% to 70% at 1 year of treatment (Additional file 1: Table S1). Current treatment guidelines advocate to consider adjunctive therapy options for DFUs that have not achieved a 50% area reduction within 4 weeks [19-21] or failed to heal after 4–6 weeks [22] of standard wound care. There are increasing number of therapeutic efforts to speed the healing of DFUs, and the literature surrounding their use is evolving [23].

From a pathophysiologic perspective, dysfunctional wound healing in diabetes is closely linked to insufficient angiogenesis [24], caused by a chronic inflammatory disposition in concert with impaired cellular responses to tissue hypoxia [25-27]. A sustained, interleukin (IL)-1β-driven prevalence of pro-inflammatory M1 macrophages associated with defective transition to reparative, granulation-promoting M2 macrophages [28-33] and an impaired activation of the hypoxia-inducible transcription factor 1α (HIF-1α) pathway by local fibroblasts and endothelial cells [34-36] leading to deficient (HIF-1α)-dependent upregulation of multiple angiogenic factors including vascular endothelial growth factor (VEGF) [34-38] ultimately result in a decreased amount of nascent microvasculature [39, 40].

In the light of a complex pathophysiology, mesenchymal stem cells (MSCs) have been considered a promising approach to adjunctive DFU treatment [41-43], owing to their remarkable ability to adaptively respond to signals associated with tissue injury and inflammation by providing paracrine signals which alter the wound environment towards a pro-healing state or even directly participate in wound regeneration [43, 44]. However, translation into clinical practice has not yet been achieved.

Recently, a skin-resident MSC population characterized by expression of ATP-binding cassette subfamily B member 5 (ABCB5) has been found severely reduced in the dermis of diabetic *db/db* mice. This might imply that the function of this cell population is impaired under diabetic conditions, which, as a consequence, might favor poor wound healing in diabetes [45]. Conversely, $ABCB5^+$ MSCs were shown to respond to inflammatory milieus through multiple cell contact-dependent and paracrine mechanisms [46-48]. In a chronic wound model mimicking human chronic venous ulcers, $ABCB5^+$ MSCs shifted the M1

macrophage prevalence toward an M2 phenotype via secretion of IL-1 receptor antagonist (IL-1RA) and rescued impaired angiogenesis in the wound bed [48]. These effects were associated with an acceleration of wound healing, which was also observed in human chronic venous ulcers treated with ABCB5$^+$ MSCs [49, 50]. Very recently, angiogenesis- and healing-promoting efficacy of ABCB5$^+$ MSCs was demonstrated also in a mouse diabetic wound model [45].

Dermal ABCB5$^+$ MSCs cells can be easily accessed from healthy human donors, expanded to a clinical scale and delivered as a good manufacturing practice (GMP)-conforming advanced-therapy medicinal product (ATMP) of proven purity, safety and tolerability [51, 52]. Aiming at developing ABCB5$^+$ MSCs for the treatment of human DFUs, we here characterize their angiogenic potential with respect to angiogenic factor expression at the mRNA and protein level, *in vitro* endothelial trans-differentiation and tube formation potential, and *in-vivo* perfusion-restoring capacity. Building upon these results in conjunction with the existing evidence on the cells' anti-inflammatory potential we have established three potency assays in order to deliver human skin-derived ABCB5$^+$ MSCs as an ATMP with standardized biological activity. Finally, this product was tested in a clinical trial in patients suffering from non-healing, standard treatment-refractory DFUs.

Methods

Expansion and isolation of human ABCB5$^+$ MSCs

Human ABCB5$^+$ MSCs were derived from skin samples obtained from patients undergoing abdominoplasties or other surgical interventions that provide left-over skin tissue after informed written consent was obtained. Cell production was carried out in an EU-GMP grade A cabinet in a grade B clean room under laminar air flow following a validated GMP-conforming protocol as described previously [51]. In brief, after enzymatic digestion of the skin tissue, cells were centrifuged and expanded as unsegregated culture by serial passaging upon adherence selection in an in-house MSC-favoring medium (Ham's F-10 supplemented with fetal calf serum, L-glutamine, fibroblast growth factor 2 (FGF-2), HEPES, hydrocortisone, insulin, glucose, and phorbol myristate acetate). ABCB5$^+$ cells were isolated by antibody-coupled magnetic bead sorting using a mouse anti-human ABCB5 monoclonal antibody directed against the extracellular loop 3 of the ABCB5 molecule [53] (Maine Biotechnology Services, Portland, Maine; GMP purification: Bibitec, Bielefeld, Germany), cryo-preserved in CryoStor® CS10 freeze medium (BioLife Solution, Bothell, WA) containing 10% dimethyl sulfoxide and stored in the vapor phase of liquid nitrogen.

Hypoxia studies

Induction of cell hypoxia

ABCB5$^+$ MSCs (3×10^5) were seeded in a culture dish and placed in a hypoxia chamber, which was flushed with nitrogen-enriched gas (1% O_2, 4% CO_2, 95% N_2) at a rate of 25–50 l/min.

HIF-1α staining

ABCB5^{+} MSCs were seeded onto coverslips, fixed with 4% paraformaldehyde solution, permeabilized with 1% Triton^{TM} X-100 (Sigma-Aldrich, Taufkirchen, Germany) in phosphate-buffered saline, blocked with 0.5% bovine serum albumin in phosphate-buffered saline, and stained for HIF-1α (for antibodies see Additional file 1: Table S2). Nuclei were counterstained with 4’,6 diamidino-2 phenylindole (DAPI) and stains microscopically (EVOS^{TM} Floid^{TM} cell imaging station; Life Technologies, Darmstadt, Germany) evaluated.

Quantitative real-time polymerase chain reaction (qPCR)

Total RNA was isolated using the RNeasy® Micro Kit (Qiagen, Hilden, Germany) and reverse-transcribed into cDNA using the Applied Biosystems^{TM} High-Capacity cDNA Reverse Transcription Kit (Thermo Fisher, Dreieich, Germany) and the Applied Biosystems^{TM} SYBR Green Mastermix (Thermo Fisher) in a four-step process run in a Mastercycler® Personal thermocycler (Eppendorf, Hamburg, Germany). PCR reactions were run in triplicate in an Applied Biosystems^{TM} StepOne RealTime^{TM} PCR System (Thermo Fisher). Primer sequences are provided in Additional file 1: Table S3. Actin served as housekeeping gene. Primer quality and integrity of the amplified product was confirmed by melting curve analysis. Identity of the PCR products was confirmed by agarose gel electrophoresis. Relative quantification of transcript levels was determined using the $2^{-\Delta\Delta Ct}$ algorithm.

Enzyme-linked immunosorbent assay (ELISA)

VEGF concentration in the cell culture supernatant was measured using the Invitrogen VEGF Human ELISA Kit (Thermo Fisher), according to the manufacturer’s instructions. Assays were run in triplicate.

Trans-differentiation studies

Angiogenic trans-differentiation assay

ABCB5^{+} MSCs (1×10^{6}) were seeded in 24-well culture plates and cultured for up to 96 h in culture medium supplemented with 200 ng/ml recombinant human (rh) VEGF (Sigma-Aldrich), 1000 ng/ml rhFGF-2 (CellGenix, Freiburg, Germany) and 1000 ng/ml rh platelet-derived growth factor-BB (PDGF-BB; R&D Systems, Wiesbaden, Germany). Trans-differentiation and proliferation activity were assessed by CD31 and Ki67 staining, respectively (for antibodies see Additional file 1: Table S2). Nuclei were counterstained with DAPI. All experiments were performed in triplicates. Human umbilical vein endothelial cells (HUVECs; 5×10^{5}; Thermo Fisher) served as positive control.

Tube formation assay

ABCB5$^+$ MSCs (1×10^5/ml or 1.5×10^5/ml) and HUVECs (0.5×10^5/ml or 1×10^5/ml) were seeded on Geltrex^{TM} (Thermo Fisher)-coated culture plates and incubated at 37°C for 19–22 h (ABCB5$^+$ MSCs) and 16–18 h (HUVECs). For examination of cell viability, cells were stained with calcein acetoxymethylester (Thermo Fisher; 1:10,000, 30 min, 37°C). Tube formation and calcein fluorescence were evaluated microscopically (EVOS^{TM} FLoid^{TM} cell imaging station).

Animal studies

Hindlimb ischemia (HLI) induction and post-surgical care

Male OF1 mice (Charles River Laboratories, Saint-Germain-Nuelles, France) were anesthetized with 2% isoflurane in 100% oxygen, and the inner faces of both hindlimbs were carefully shaved. After local disinfection, an about 1-cm skin incision was made on the left hindlimb from the inguinal region to the bifurcation region of the femoral artery into the saphenous and popliteal artery. The femoral artery and vein were dissected from the nerve. The femoral artery/vein block was ligated proximally by two 8-0 ties placed just distally from the superficial epigastric artery, and distally by two 8-0 ties placed just proximally from the bifurcation of the femoral artery into the saphenous and the popliteal artery. After cutting the femoral artery/vein block between the two proximal and between the two distal ties, the femoral artery/vein block was removed. When necessary, major branches such as the lateral circumflex femoral artery were ligated to avoid bleeding.

Thereafter, subcutaneous tissue and skin were closed with non-resorbable sutures or clamped with titanium micro clips (WDT, Garbsen, Germany). Postoperative care included pain management by injection of buprenorphine (Buprenovet, Bayer; 0.1 mg/kg) once directly after surgery or flunixin meglumine (2.5 mg/kg twice daily) during 3 days and daily local wound care with an antiseptic healing cream (Dermaflon, Pfizer).

Injection of ABCB5$^+$ MSCs

On the day after surgery, mice were anesthetized with isoflurane to receive intramuscular injections at the ischemic limb of human ABCB5$^+$ MSCs suspended in Ringer's lactate solution containing 2.5% human serum albumin and 0.4% glucose at concentrations between 1×10^6 and 1×10^8 cells/ml, as required. Cell doses, injection volumes and sites are given in the *Results* section.

Blood perfusion measurement

Animals were anesthetized with isoflurane and placed on a warming platform in a supine position for imaging at the internal face of the thighs. Hindlimb blod flow was measured before and immediately after surgery (day 1) and on days 3, 5, 7, 14, 21 and 28 by real-time laser doppler blood perfusion imaging (LDPI; PeriCam PSI, Perimed Instruments). The scanned area covered an ellipse framing internal face of the thigh. Blood perfusion was expressed as the ratio between LDPI values in the left (ischemic) and right (non-ischemic) limb.

Histopathology and immunohistochemistry

Animals were sacrificed by CO_2 inhalation and the thigh and gastrocnemius muscles preserved in 10% neutral buffered formalin solution, which was replaced after 24–48 h by 70% ethanol. Fixed tissues wee embedded in paraffin wax, cut to 2–4 µm thickness, stained with hematoxylin and eosin, and inspected by conventional light microscopy. Neovascularization was semi-quantitatively quantified as 0 = none, 1 = minimal capillary proliferation, focal, 1–3 buds, 2 = groups of 4–7 capillaries with supporting fibroblastic structures, 3 = broad band, and 4 = extensive band of capillaries with supporting fibroblastic structures. Immunohistochemical staining for CD31 was performed using rabbit anti-human/mouse CD31 (ab28364, Abcam; dilution 1:50) and dextran polymer-horseradish peroxidase-labelled anti-rabbit IgG (DAKO EnVision®+, K4010, Agilent) for detection. CD31 expression was semi-quantitatively quantified as 0 = none, 1 = minimal, 2 = slight, and 3 = moderate by two independent investigators who were blinded to the treatment.

Statistics

One-way ANOVA followed by Dunnett's test was used to compare LDPI ratios within versus baseline and neovascularization and CD 31 expression in the cell-treated groups versus control.

Clinical trial

Patients

Adults (18–85 years) with diabetes mellitus type 2 (hemoglobin A1c <11%) were eligible if they had a neuropathic diabetic plantar foot ulcer (Wagner grade 1 or 2, 1–50 cm^2), confirmed by vibration sense testing (128-Hz Rydel-Seiffer tuning fork) without presence of significant arterial disease (ankle-brachial index ≥0.7 or transcutaneous oxygen pressure >40 mmHg or as per Doppler ultrasonography).

Main exclusion criteria were acute Charcot foot, active osteomyelitis, treatment-requiring ulcer infection, adjacent or chronic skin disorders, skin malignancies, acute or untreated deep vein thrombosis, need for hemodialysis, surgical procedures within 2 months and use of active wound care agents within 2 weeks prior to treatment, and current use of systemic immunosuppressants, cytotoxics or glucocorticoids.

Trial design

The study was a national, multicenter (eight sites in Germany), open-label, single-arm, phase I/IIa trial comprising three periods: standard-of-care screening (≥ 6 weeks), treatment and efficacy follow-up (weeks 1–12), and safety follow-up period (until end of month 12). The trial was performed in accordance with the Declaration of Helsinki and local regulations and approved by the ethical committees of all participating study sites. Patients gave written informed consent prior to trial participation.

Interventions

Treatment consisted of up to two topical applications of 2×10^6 allogeneic ABCB5$^+$ MSCs (suspended in Ringer's lactate solution containing 2.5% human serum albumin and 0.4% glucose [51]) per cm^2 wound area on day 0 and at week 6. The cells were manufactured as a GMP-conforming standardized ATMP (for main product release data see Additional file S1: Table S4). Originally, only one cell application was planned. The second application was amended to the protocol only after data from a first-in-human trial on chronic venous ulcers [49] suggested that a second cell dose at 6 weeks after the first cell dose might provide additional benefit for chronic wound healing. Cell application could be preceded by an optional wound debridement at the investigator's discretion followed by waiting until the bleeding had entirely stopped. For cell application, a suspension containing 1×10^7 ABCB5$^+$ MSCs/ml was applied onto the wound surface, delivering 2×10^6 ABCB5$^+$ MSCs/cm^2 wound surface area. Thereafter, the cells were allowed to settle for 15–30 min, optionally fixed in place with fibrin gel (Tisseel®; Baxter, Unterschleißheim, Germany), and then the wound was covered with a waterproof film dressing (Tegaderm™; 3M, Neuss, Germany). On the following day (≥ 12 hours after cell application), the film dressing was replaced by a microbe-binding dressing (Cutimed® Sorbact® tamponade or compress; BSN, Hamburg, Germany), which was changed again 1–2 days later. Additionally, patients received standard care until week 12 including glycemic control, ulcer debridement, appropriate wound dressings (*i.e.* microbe-binding tamponade of cavities and exudate-absorbent foam dressing for coverage), and antibiotics if required. All patients had to use offloading devices including cast devices or individually fitted therapeutic footwear [19, 54, 55].

Outcome measures

Primary efficacy endpoint was percent wound surface area reduction at week 12 or last available post-baseline measurement. Secondary efficacy endpoints were percent and absolute wound surface area reduction at predefined visits, proportion of patients achieving complete and 30% wound closure, time to complete and to 30% wound closure, granulation, epithelialization, wound exudation, time to amputation at the target leg, pain and life quality. Safety outcome measures included adverse events (during the

whole study period) and vital signs, changes in physical examination findings and time to amputation of the target leg (during efficacy follow-up).

Outcome determination

Wound surface area determination followed a multi-step approach combining computerized evaluation (PictZar® planimetry software; BioVisual, Elmwood Park, NJ, USA; 98% accuracy, 94% inter-rater reliability, 98% intra-rater reliability according to a validation and reliability study [56]) of standardized photographs and depth measurements using a wound measuring probe, to account for the typical three-dimensional shape of DFU wounds; *i.e.* consisting of wound floor, side wall and, occasionally, not visible tunneling or undermining areas. For details of the measuring and calculation algorithm see Additional file 2: Methods S1. Formation of granulation and epithelial tissue was estimated by the investigator in % of wound area from standardized wound photographs. Wound exudation was rated by the investigator as low (dry), moderate (moist), and high (wet) according to the criteria defined by the World Union of Wound Healing Societies [57]. Pain was rated by the patient using a 0–10-point numerical rating scale with 0 = no and 10 = worst imaginable pain. Quality of life was assessed using the participant-reported Short Form (36) Health Survey (SF-36) and Dermatology Life Quality Index (DLQI) questionnaires.

Sample size

Enrolment followed a Simon optimal two-stage design with responders defined as patients presenting with at least 30% wound surface area reduction at week 12. The sample size required to achieve 80% power at 5% significance level was calculated using PASS 13 software (NCSS, East Kaysville, UT, USA) to be 37 patients. This enabled the option to terminate the trial if ≤ 6 or ≥ 14 of the first 18 treated patients were responders. As in an interim analysis 12 of 18 patients emerged as responders, recruitment was continued. However, by force of the emerging COVID-19 pandemic, the trial was prematurely completed. At that time, 23 patients had been treated.

Statistical analysis

Safety assessments were performed on the safety analysis set, which included all patients who received at least one cell dose. Efficacy assessments were performed on the full analysis set (FAS), which included all patients of the safety analysis set who underwent wound surface area assessments at baseline and at least one post-baseline visit, and on the per-protocol set (PP), which included all patients of the FAS who had no major protocol deviations.

If not otherwise stated, normally (D'Agostino–Pearson normality test) distributed parameters are presented as mean ± standard deviation, and non-normally distributed parameters as median and interquartile range (IQR). Statistical significance of percent wound surface area changes from baseline

was tested against the null hypothesis (median change = 0) using a two-sided Wilcoxon signed rank test. Time to complete wound closure, time to 30% wound surface area reduction and time to amputation at the target leg were analyzed using the Kaplan–Meier method.

Results

Hypoxia studies

Hypoxia-induced HIF-1α activation in ABCB5$^+$ MSCs

Prior to hypoxic incubation, HIF-1α protein was mainly detectable in the cytoplasm. During hypoxic incubation, cytoplasmic HIF-1α fluorescence decreased while nuclear HIF-1α fluorescence increased. At 24 h of hypoxia, HIF-1α was mainly detectable in the nuclei, indicating that nuclear translocation has occurred (Fig. 1A). In contrast, on the transcriptional level, HIF-1α mRNA expression peaked after 1 h of hypoxic culture and decreased thereafter, dropping down to roughly 10% of the baseline value at 48 h (Fig. 1B).

Hypoxia-induced VEGF mRNA expression and protein secretion in ABCB5$^+$ MSCs

During hypoxia, VEGF mRNA expression increased about fourfold from baseline at 5 h, remaining on that level during 48 h (Fig. 1C). VEGF protein secretion steadily increased during 48 h of hypoxic culture (Fig. 1D).

Angiogenic potency assay

The VEGF ELISA after hypoxic culture was used as a surrogate potency assay to predict the pro-angiogenic bioactivity of GMP-compliantly produced ABCB5$^+$ MSCs for use in clinical trials. Since VEGF secretion was highest at 48 h of hypoxic culture (Fig. 1D), the 48-h time point was set as temporal endpoint for potency testing. In validation studies (not shown), a VEGF concentration in the supernatant of ≥46.9 pg/ml, corresponding to an optical density threshold <3.0 in the serial standard dilution of the ELISA kit, was validated to reliably enable qualitative detection and, therefore, defined as acceptance criterion for cell batch release. For the potency data of the cell batches used in the present clinical trial see Additional file S1: Table S4.

Trans-differentiation studies

Growth factor-stimulated endothelial trans-differentiation

After 96 h culture in medium supplemented with 200 ng/ml VEGF, 1000 ng/ml FGF-2 and 1000 ng/ml PDGF-BB, ABCB5$^+$ MSCs underwent endothelial trans-differentiation as revealed by CD31 expression (Fig. 2A-C). Trans-differentiation was accompanied by an enhanced proliferative activity as evidenced by Ki-67 staining (Fig. 2D-F).

Tube formation on gel matrix

After 18–20 h cultivation on Geltrex^{TM} gel matrix, ABCB5$^+$ MSCs formed capillary-like structures similar to HUVECs that were used as positive-control. The tubular structures stained positive for calcein, demonstrating viability (defined as metabolic activity measured by conversion of calcein acetoxymethylester to calcein) of the tube-forming cells (Fig. 3).

Trans-differentiation potency assay

The tube formation assay was used as a surrogate potency assay to predict the trans-differentiation capacity of GMP-compliantly produced ABCB5$^+$ MSCs for use in clinical trials. For grading, tube formation of ABCB5$^+$ MSCs was semi-quantitatively classified into six categories ranging from 1 = tubular branches of several cells forming a defined network-like structure to 6 = no tubular branches visible (for a more detailed description of all categories see Additional file S1: Table S4, with ≤3 in at least one of the two seeded cell concentrations (1×10^5/ml and 1.5×10^5/ml) being considered as successful angiogenic differentiation. For the potency data of the cell batches used in the present clinical trial see Additional file S1: Table S4.

Animal studies

Blood flow recovery in surgically induced HLI

Mice (n = 10 per group) received 5×10^6 ABCB5$^+$ MSCs/animal or vehicle only by intramuscular injection (200 µl injection volume split over 4 injection sites at the internal face of the thigh) at 24 h after HLI induction. During the study, a certain mortality (day 3, 10%; day 5, 20%; day 7, 25%) was observed, which did not differ between groups. Blood perfusion measured by LDPI (Fig. 4A) and expressed as ratio between LDPI values in the ischemic and the non-ischemic limb (Fig. 4B) significantly decreased immediately after surgery in both treatment groups. During the following days the LDPI ratio gradually recovered, reaching baseline levels on day 5 in the MSC-treated group as compared to day 14 in the vehicle-treated group, with the most pronounced difference in LDPI ratio between groups occurring between days 5 and 7 (Fig. 4B).

CD31 expression in surgically induced HLI

Mice (n = 10 per group) received 5×10^5, 1×10^6 or 5×10^6 ABCB5$^+$ MSCs/animal or vehicle by intramuscular injection (200 µl injection volume split over 4 injection sites at the internal face of the thigh) at 24 h post HLI induction. At day 6, semiquantitative immunohistochemical evaluation revealed a significant increase in mean CD31 expression in the left thigh muscles of mice treated with the two higher cell doses as compared to the vehicle group (Fig. 4C).

Neovascularization in surgically induced HLI

Mice received 1×10^5, 5×10^6 or 1×10^7 ABCB5$^+$ MSCs/animal (n = 7 per group) or vehicle (n = 6) by intramuscular injection (100 µl injection volume split over 5 injection sites at the quadriceps, semitendinosus and gastrocnemius muscles) at 24 h post HLI induction. At day 6, semiquantitative histological evaluation revealed a significant increase in the mean neovascularization score in the left (ischemic) gastrocnemius muscles of mice treated with the highest cell dose as compared to the vehicle group (Fig. 4D, E).

Clinical trial

Progress of the study

Patients were enrolled between November 2017 and January 2020. Forced by the COVID-19 pandemic, which was associated with critical issues including staffing shortages, impairments of supply chains and increased infection risk for the elderly and/or comorbid study patients, recruitment and treatment were discontinued as of April 2020, and the trial was prematurely completed as of end of June 2020 after consultation with the ethics committee and the regulatory authority. At that time, all treated patients had completed the efficacy follow-up. Patients who had entered the safety follow-up period but were not scheduled for a safety visit in June 2020 were subjected to a supplementary end-of-study visit (Fig. 5A, B).

Patients

Totally 63 patients were screened, of which 23 patients (20 men, 3 women) were treated (Fig. 5B). During the screening period, which ranged from 42 to 68 days (one outlier: 118 days; median: 49 days), changes in wound surface area ranged from 56% decrease to 175% enlargement (median change 0%) (Fig. 5C). Baseline characteristics of the treated patients are listed in Table 1.

Table 1

Baseline characteristics of all treated patients

Variable		Full analysis set (N=23)
Age, years	Median (range)	62 (49–79)
Sex		
male	n (%)	20 (87)
female	n (%)	3 (13)
Body weight, kg	Median (range)	105 (71–141)
Body mass index, kg/m^2	Median (range)	33 (26–44)
Target wound surface area, cm^2	Median (range)	2.6 (1.0–15.2)
Ankle-brachial index	Median (range)	1.1 (0.8–2.0)
Hemoglobin A1c, %	Median (range)	7.2 (5.0–9.8)

Of the 23 treated patients, 7 patients received only one cell application: 3 patients because they had been enrolled under earlier protocol versions before the second application was amended to the protocol, two patients because their wounds were already closed at the week-6 visit, one patient due to a (not treatment-related) foot fracture, and one patient due to COVID-19 pandemic-related treatment discontinuation. One patient was lost to follow-up after the month-9 safety visit (Fig. 1B). Three patients had major protocol deviations: use of prohibited medication (active wound care agent), delayed week-12 visit, improper off-loading. These patients were analyzed in the FAS (N=23) but excluded from the PP (N=20).

Efficacy outcomes

The wound healing progress of three representative responders is illustrated in Fig. 6. The primary efficacy outcome, median wound surface area reduction from baseline at week 12, was 59% (IQR: 27-96%, FAS) and 64% (IQR: 46-96%, PP) (p<0.001 in both sets) (Fig. 7A-C).

A summary of the secondary efficacy outcomes is given in Table 2.

Table 2

Summary of the main secondary efficacy outcomes

Parameter	Full analysis set (N=23)	Per-protocol set (N=20)	Source[a]
Absolute wound surface area reduction			
Change from baseline at week 12 (cm^2)[b]	1.7 (0.3–2.8)	2.0 (0.9–2.9)	Table S5
Complete wound closure			
Patients with complete closure at week 12, n (%)	6 (26)	6 (30)	Table S6
Patients with complete closure at any time up to week 12, (%)	6 (26)	6 (30)	Table S6
Time to complete closure, days[c]	Not reached	Not reached	Fig. 7C
≥30% wound surface area reduction			
Patients with ≥30% reduction at week 12 (“Responders”), n (%)	17 (74)	17 (85)	Table S6
Patients with ≥30% reduction at any time up to week 12, n (%)	19 (83)	18 (90)	Table S6
Time to ≥30% reduction, days[c]	27 (14; 30)	22 (14; 30)	Fig. 7D
Reopening after complete wound closure			
Patients with wounds reopened at week 12, n (%)	0 (0)	0 (0)	n.a.
Exudation			
Wounds with low exudation, n (%)			
Day 0	10 (44)	7 (35)	Table S7
Week 12	12 (52)	10 (50)	Table S7
Wounds with moderate exudation, n (%)			
Day 0	11 (48)	11 (55)	Table S7
Week 12	10 (44)	9 (45)	Table S7
Amputation at target leg			
Patients with amputation, n (%)	1 (4)	1 (5)	n.a.
Time to amputation, days	42	42	n.a.
Pain score[b]			
Day 0	1 (0–3)	n.a.	Table S8
Week 12	1 (0–2)	n.a.	Table S8

Quality of life[d]			
Dermatology Life Quality Index[b]			
Day 0	6 (1–12)	n.a.	Table S9
Week 12	4 (0–10)	n.a.	Table S9

n.a. not applicable

[a]Detailed results are given in Additional file 1: Tables S5–S9

[b]Median (interquartile range)

[c]Median (95%-CI)

[d]Due to space limitations, SF-36 subscale scores (which remained virtually unchanged during the efficacy follow-up) are not shown here but given in Additional file 1: Table S9

The median percentage wound surface area reduction was already statistically significant (p<0.001) at 2 weeks and, except for the week-6 assessment (which was, however, missed by 4 patients), increased further over time (Fig. 7A, B).

Absolute wound surface area reduction was most pronounced during the first 2 weeks after the first and second MSC application, *i.e.* from day 0 till week 2 and from week 6 till week 8, respectively (Additional file 1: Table S5).

Complete wound closure was achieved in 6 patients (26% for FAS and 30% for PP; Additional file 1: Table S6). Since less than half of patients experienced complete wound closure during the efficacy follow up, the median time to complete wound closure could not be determined (Fig. 7D).

Wound surface area reduction by at least 30% at week 12 was observed in 17 patients (74% for FAS and 85% for PP) (Additional file 1: Table S6). These patients were considered responders. The median time to first 30% wound surface area reduction was 27 days (95%-CI: 14; 30; FAS) and 22 days (95%-CI: 14; 30; PP) (Fig. 7E).

Due to the nature of DFU morphology, formation of granulation and epithelial tissue was not reliably evaluable.

Most patients demonstrated low or moderate wound exudation. The proportions of patients with low, moderate or high exudation varied slightly over time with a few more patients having low exudation at week 12 than on day 0 (52% vs. 44% and 50% vs. 35% for FAS and PP, respectively) (Additional file 1: Table S7).

An amputation at the target leg until week 12 was reported in one patient. The reason was a fracture of the little toe, which the investigator judged as unrelated to the cell therapy. Since only one patient experienced an amputation during the efficacy follow up, the median time to amputation could not be calculated.

Median pain score was low during the whole 12-week follow-up period (Additional file 1: Table S8). The SF-36 subscale scores remained virtually unchanged, while the median DLQI slightly improved from 6 (1–12) at day 0 to 4 (0–10) at week 12 (Additional file 1: Table S9).

Post-hoc analyses

Wound size analyses were additionally performed on the subgroup of responders, *i.e.,* all patients who presented with ≥30% wound surface area reductions from baseline at week 12. Baseline patient characteristics, percent change of wound surface area during screening and baseline wound size did not differ between the responders and the non-responders (Fig. 8A, B). All except three responders had achieved first 30% wound surface area reduction within 30 days; median time to first 30% wound surface area reduction was 16 days (Fig. 7E). At week 12, median wound surface area reduction from baseline was 67% (55%–98%) (Fig. 7C), and in 6 of 17 (35%) responders the wound had fully closed.

Since in the trial protocol no threshold values had been specified to exclude patients from study treatment based on their wound surface area changes during the screening period, a Spearman's rank correlation analysis was performed to test whether there was an association between wound surface area reduction during the screening period and during the efficacy follow-up period. A Spearman's rank correlation coefficient of 0.007 (95% CI = -0.429, 0.417; p=0.97) indicated that there was no association between these two parameters (Fig. 8C).

Safety outcomes

During the whole study period, 93 treatment-emergent adverse events (TEAEs) were reported in 20 of 23 patients (Table 3). Most TEAEs were mild or moderate; 3 TEAEs reported by two patients were severe. Twelve TEAEs reported by 10 patients were serious (Additional file 1: Table S10). None of the TEAEs was judged related to the cell product.

Table 3

Adverse events (SAS)

Event	Number of events	Number (%) of patients
Any adverse event[a]	120	21 (91)
Any TEAE	93	20 (87)
Any serious TEAE	12	10 (43)
Any treatment-related TEAE	0	0 (0)
Frequent TEAEs by MedDRA system organ class[b]		
General disorders and administration site conditions		**3 (13)**
Oedema peripheral		2 (9)
Infections and infestations		**15 (65)**
Infected skin ulcer		6 (26)
Localized infection		4 (17)
Nasopharyngitis		4 (17)
Wound infection		2 (9)
Injury, poisoning and procedural complications		**5 (22)**
Ligament sprain		2 (9)
Metabolism and nutrition disorders		**4 (17)**
Hyperglycemia		2 (9)
Musculoskeletal and connective tissue disorders		**4 (17)**
Arthralgia		2 (9)
Back pain		2 (9)
Pain in extremity		3 (13)
Skin and subcutaneous tissue disorders		**11 (48)**
Blisters		6 (26)
Skin ulcer		4 (17)

MedDRA Medical Dictionary for Regulatory Activities; *TEAE* Treatment-emergent adverse event; *SAS* Safety analysis set (N=23)

[a]Includes pretreatment-emergent (occurring between giving written consent and first cell application) and treatment-emergent (occurring between first cell application and end of safety follow-up) adverse events

[b]Only TEAEs that were reported by at least 2 patients

During efficacy follow-up, no clinically relevant changes in vital signs occurred (Additional file 1: Table S11). Eighteen physical examination findings that were either not present at baseline or had changed versus baseline were documented in 10 patients (Additional file 1: Table S12). Of these, 10 findings (56%) represented improvements.

Discussion

Despite well-established strategies for DFU management, treatment is often challenging, and many patients respond only poorly to standard treatment. Experimental approaches that directly target defective pathways in the wound tissue, including blockade of IL-1β by a neutralizing antibody or IL-1RA [30, 58, 59], stabilization of HIF-1α using prolyl hydroxylase inhibitors, iron chelator or protein-protein interaction inhibitors [35, 37, 60, 61] or topical supplementation of pro-angiogenic growth factors [39, 62], have accelerated wound healing in diabetic mice. However, the clinical translation of these approaches has been hampered by various hurdles including safety concerns, short half-lives and/or the requirement of specific delivery systems [61, 63, 64]. In contrast to single-drug approaches, therapeutically applied MSCs are considered, by sensing their environment for hypoxia or other stress signals and making use of multiple pathways, to respond more accurately according to the physiological needs [43, 44].

Here we demonstrate that skin-derived ABCB5$^+$ MSCs adaptively activate the proangiogenic HIF-1 pathway in response to hypoxic conditions. Activation occurred through posttranslational stabilization of HIF-1α protein (which at normoxia is subject to rapid degradation), which resulted in cellular accumulation and translocation to the nucleus (Fig. 1A). HIF-1α pathway response to hypoxia became also evident at the transcriptional level, albeit with different kinetics: Whereas HIF-1α protein accumulation and nuclear translocation was most pronounced at 24 h, HIF-1α mRNA levels, after initial upregulation to peak levels already at 1 h, progressively decreased during sustained hypoxia, having returned to baseline levels at 5 h and dropping further thereafter (Fig. 1B). Similar kinetics of HIF-1α mRNA expression in response to hypoxia have been observed in various cell types including endothelial cells and have been ascribed to a negative feedback loop that counteracts excessive HIF-1α protein accumulation during prolonged hypoxic conditions [65]. Interestingly, in mice transplanted with subcutaneous gel grafts cellularized with MSCs and endothelial progenitor cells (EPCs), genetic ablation or pharmacologic inhibition of HIF-1α in the MSCs completely abrogated experimental vessel formation in the gel graft, while HIF-1α deletion in the EPCs had no effect on vasculogenesis [66]. Thus, even though HIF-1α pathway activation is basically a common mechanism by which a cell adapts to reduced oxygen tension, HIF-1α stabilization in MSCs was considered a crucial event in cell-based therapeutic vasculogenesis [66]. In ABCB5$^+$ MSCs, HIF-1 pathway activation was accompanied by about fourfold upregulation of VEGF transcription (Fig. 1C), which eventually resulted in a substantial increase in VEGF protein secretion (Fig. 1D).

In addition to paracrine VEGF secretion under hypoxic conditions, ABCB5$^+$ MSCs proved capable of adopting phenotypic and functional characteristics of endothelial cells *in vitro*, as demonstrated by

expression of CD31 when cultured in growth factor-supplemented medium (Fig. 2A) and formation of capillary-like structures similar to HUVECs when seeded on gel matrix (Fig. 3). This suggests that ABCB5$^+$ MSCs can trans-differentiate into endothelial-lineage cells, and might imply that, beyond serving paracrine proangiogenic functions to promote vascular regeneration, ABCB5$^+$ MSCs could even directly participate in neoangiogenesis in the injured tissue. Previously, ABCB5$^+$ MSCs have shown superior homing and engraftment to mouse skin wounds as compared to bone marrow-derived MSCs [67]. Graft survival was demonstrated in the skin against a fully allogeneic barrier (BALB/c ABCB5$^+$ MSCs administered to C57/BL6 mice) for at least 17 days [46]. Moreover, in an NSG mouse wound model, significant detection of human-specific CD31 DNA in the wound tissue at 13 days after topical application of human ABCB5$^+$ MSCs has indicated that endothelial trans-differentiation of these cells can actually occur *in vivo* [49]. Still, whether therapeutically applied ABCB5$^+$ MSCs indeed become integrated in the regenerating vasculature remains to be elucidated.

To investigate the vascular regenerative potential of ABCB5$^+$ MSCs *in vivo*, we studied the effects of intramuscular cell injection on perfusion restoration in a mouse HLI model. In this model, ABCB5$^+$ MSCs markedly accelerated perfusion recovery as measured by LDPI (Fig. 4B). At the microscopic level, ABCB5$^+$ MSCs increased the vascularization assessed by CD31 immunostaining (Fig. 4C) and enhanced the proliferation of capillaries in the ischemic muscles (Fig. 4D, E).

Beside proangiogenic capacity based on paracrine activity and endothelial differentiation, a third principal mode of action by which MSCs perform their effects over injured tissue is through interaction with the immune system. While immune modulation has not been addressed in the present study, previous studies have demonstrated that ABCB5$^+$ MSCs respond to inflammatory milieus through multiple cell contact-dependent and paracrine mechanisms [46-48], including dampening the IL-1β-driven inflammation in chronic wounds by adaptive IL-1RA release, thereby shifting the prevalence of M1 toward proangiogenic and repair-promoting M2 macrophages in the wound tissue [48].

With respect to these three principal modes of actions we have developed and established three potency assays to guarantee biological functionality and predict clinical effectiveness of therapeutically applied ABCB5$^+$ MSCs: (i) VEGF secretion under hypoxic conditions to evaluate the angiogenic potency, (ii) tube formation on extracellular matrix gel to evaluate the endothelial trans-differentiation capacity, and (iii) IL-1RA secretion after cocultivation with M1-polarized macrophages to evaluate the immunomodulatory potency (Additional file S1: Table S4).

Based on the *in-vitro* and preclinical observations we investigated ABCB5$^+$ MSCs as a potential option for adjunctive treatment of DFUs. In the patient population studied, the greatest treatment success achieved over the ≥6-week screening period (median 7 weeks) with standard care alone was approximately 50% wound surface area reduction in 3 of 23 patients (of whom 1 patient was even treated 118 days), while in about half of the patients the ulcer enlarged (up to 175%) (Fig. 5C). Thus, in line with current DFU treatment guidelines, which recommend to consider adjunctive therapy options for DFUs that did not

achieve a 50% area reduction within 4 weeks [19-21] or failed to heal after 4–6 weeks [22] of standard treatment, these ulcers had appeared refractory to standard treatment, indicating an urgent need for an advanced wound closure strategy [19-22, 68].

In this hard-to-heal population, adjunctive topical application of ABCB5^{+} MSCs elicited statistically significant median wound surface area reductions from baseline of 59% (FAS), 64% (PP) and 67% (subgroup of responders) after 12 weeks. Acceleration of wound healing started early, becoming statistically significant ($p<0.001$) already at 2 weeks (median wound surface area reduction 31% for FAS and PP) (Fig. 7A, B), which indicates that as early as at 2 weeks about half of the patients (48% of FAS and 56% of PP) had passed the predefined threshold value of 30% wound surface area reduction that was considered to classify them as responders (Fig. 7D). At 4 weeks, the median wound surface area reduction was 44% (FAS) and 48% (PP), and 1 patient (4% of FAS and 5% of PP) presented already with full wound closure (Fig. 7A, B), which together revealed that the overall situation had clearly improved as compared to the standard-of-care screening period. Finally, at week 12, 6 of these urgent-need patients (26%, 30% and 35% of FAS, PP and responders, respectively) had reached full wound closure, and it seems reasonable to expect that this rate would increase further if the follow-up period was extended, as suggested by the observation that the median wound surface area reduction was still increasing (Fig. 7A, B).

In view of the high personal and socioeconomic disease burden of DFUs it has become desirable to identify the patients who are likely to benefit from an adjunctive treatment strategy as early as possible. Basically, the phenomenon that a certain proportion of patients do not respond to the treatment, is widely known across the various MSC therapy approaches in a broad range of diseases, with non-responders potentially amounting up to 60% of the treated patients [69]. A major part of variability in clinical outcomes of MSC therapies has been ascribed to heterogenous products with insufficiently characterized therapeutic potency [70]. In contrast, in the present study, the strongly standardized quality and potency of the cell product (Additional file S1: Table S4) rules out potential differences in quality and bioactivity as a cause of variation in the treatment responses, which is supported by the comparably low non-responder rates of 26% (FAS) and 15% (PP). Importantly, there was no association between the treatment responses and the potency assay data of the applied cells (Additional file S1: Table S4), which indicates that the specified threshold acceptance values for product release are strong enough to guarantee proper biological activity. When comparing potential patient-related negative predictors for DFU healing such as greater wound surface area [71-76] and patient characteristics including older patient age [76-78], male gender [74, 79], very high [80] or very low [78] body mass index, lower ankle-brachial index [79] and lower hemoglobin A1c [81], there were no significant differences between the responders and the non-responders that seem to have contributed to failure of treatment response (Fig. 8A). Clearly, however, the etiology of impaired DFU healing is far more multi-factorial, involving, e.g., previous diabetes control, comorbidities, and psycho-social factors [68]. On a cellular level, differential regulation or variations of genes involved in skin barrier function, inflammation or vascularization and blood flow have been associated with impaired DFU healing [82-85]. To further investigate what segregates responders to

ABCB5$^+$ MSC treatment from non-responders could aid identifying predictors of response which might help distinguishing already before treatment initiation the patients that will likely respond to ABCB5$^+$ MSC therapy from those who will not.

Naturally, the conclusions drawn from the present trial are limited by factors typically associated with early-phase trials, particularly a small patient number and an open, non-randomized design. Even though all ulcers had emerged refractory to standard treatment, we cannot rule out that part of the observed improvements has occurred through additional attention and care during the trial. Not least, as discussed above, wound healing can be influenced by various patient-specific factors that were not controlled for.

Despite these limitations we conclude that the present results support GMP-manufactured dermal ABCB5$^+$ MSCs as a potential developable candidate for adjunctive therapy of standard treatment-refractory DFUs, even though in the present trial the majority of responders achieved only partial wound closure. Clearly, partial wound closure is a clinically less meaningful outcome than full wound closure; however, it is considered valid to “indicate relevant biological activity and help guide subsequent trials design” [86]. Importantly, the absence of any treatment-related adverse event during the trial confirmed good tolerability and overall safety of the cell product.

Conclusion

The present studies demonstrate the *in vitro* and *in vivo* angiogenic potential of ABCB5$^+$ MSCs based on both, paracrine pro-angiogenic factor secretion and trans-differentiation into endothelial-lineage cells. Together with the wound surface area reduction observed upon topical administration onto chronic DFUs, the results support GMP-manufactured ABCB5$^+$ MSCs as a safe, viable candidate for adjunctive therapy of treatment-refractory DFUs and warrant further investigation in a larger randomized controlled trial with a dose-ranging design, an extended efficacy follow-up period and advanced outcome measures in order to validate the benefit and optimize the dose regime.

Abbreviations

ABCB5: ATP-Binding Cassette Transporter, Subfamily B, Member 5

ATMP: Advanced-therapy medicinal product

DAPI: 4’,6 Diamidino-2 phenylindole

DFU: Diabetic foot ulcer

DLQI: Dermatology Life Quality Index

ELISA: Enzyme-linked immunosorbent assay

FAS: Full analysis set

FGF-2: Fibroblast growth factor 2

GMP: Good Manufacturing Practice

HIF-1: Hypoxia-inducible transcription factor 1

HLI: Hindlimb ischemia

HUVEC: Human umbilical vein endothelial cells

IL-1β: Interleukin 1β

IL-1RA: IL-1 receptor antagonist

IQR: Interquartile range

LDPI: Laser doppler blood perfusion imaging

MSC: Mesenchymal stem cell

PDGF-BB: platelet-derived growth factor-BB

PP: Per-protocol set

qPCR: Quantitative real-time polymerase chain reaction

rh: Recombinant human

SF-36: Short Form (36) Health Survey

TEAE: Treatment-emergent TEAE

VEGF: Vascular endothelial growth factor

Declarations

Ethics approval and consent to participate

Skin samples were obtained in accordance with the German Medicines Act (“Arzneimittelgesetz”) and the German Act on Organ and Tissue Donation, Removal and Transplantation (“Transplantationsgesetz”) and its amending tissue regulation (TPG-GewV) as discard tissues from plastic surgeries from donors who had given written informed donor consent.

All animal experiments were performed by two specialized contract research organizations complying with the requirements defined in European regulations [87] and the applicable national (French and

German) animal welfare legislations. The experimentation procedures had been approved by the Ministère de l'Enseignement Supérieur de la Recherche et de l'Innovation, France (APAFIS 2015090212419040), and the Brandenburg State Office for Environment, Health and Consumer Protection, Germany (V3-2347-A-13-8-2011), respectively.

The clinical trial was conducted according to the principles of the Helsinki Declaration and Good Clinical Practice. The protocol and all other relevant documents was approved by the local independent ethics committees (lead committee: Ethics Committee at the University of Würzburg, Würzburg, Germany; reference number 64/17_ff-sc) and the competent regulatory authority (Paul Ehrlich Institute, Langen, Germany; reference number 3034/01). Prior to any trial-related activities or procedures, all patients gave written informed consent.

Consent for publication

All patients have consented to publication of their data and images.

Availability of data and materials

The datasets generated and/or analyzed during the current study are available from the corresponding author on reasonable request. For requests regarding ABCB5 monoclonal antibody availability contact Markus H. Frank, Markus.Frank@childrens.harvard.edu.

Competing interests

MHF and NYF are inventors or co-inventors of US and international patents assigned to Brigham and Women's Hospital and/or Boston Children's Hospital (Boston, MA, USA), licensed to TICEBA GmbH (Heidelberg, Germany) and RHEACELL GmbH & Co. KG (Heidelberg, Germany). MHF and KSK serve as scientific advisors to TICEBA and RHEACELL and participate in corporate-sponsored research collaborations with RHEACELL. ENR, SK, JE, SS and SB are employees of TICEBA. KD, KK and HMS are employees of RHEACELL. CG is CEO, and MAK is CSO of TICEBA and RHEACELL. The remaining authors declare no competing interests.

Funding

AK was supported by the Interdisziplinäres Zentrum für Klinische Forschung (IZKF) Würzburg (AdvCSP-2). Contributions by NYF and MHF to this work were supported by National Institutes of Health (NIH)/National Eye Institute (NEI) grants RO1EY025794 and R24EY028767and National Heart, Lung, and Blood Institute (NHLBI) grant 1R01HL161087. KSK was supported by the German Research Foundation (DFG) within the Collaborative Research Center (CRC) 1149 Trauma.

Authors' contributions

AK made substantial contributions to the design of the clinical trial, reviewed the manuscript, and served as coordinating principal investigator of the clinical trial. KD organized and supervised the clinical trial.

ENR compiled and visualized the data and wrote the manuscript. SK performed and analyzed the trans-differentiation studies and contributed substantially to the development of the tube formation assay. MJ, CH, GD, LS, UMP, KS, GK and TR served as site principal investigators of the clinical trial. KK served as project manager of the clinical trial. JE implemented and ensured GMP compliance of the manufacturing process of the ABCB5$^+$ MSCs. HMS contributed to the design of the preclinical and clinical trials and to data visualization. SS managed the quality control and release procedures of the ABCB5$^+$ MSCs. SB managed the manufacturing of the ABCB5$^+$ MSCs. MGo, MGa, AMG, GFM, DPO and NYF made substantial contributions to the conception of the studies and the design of the clinical trial. CG, KSK and MHF contributed substantially to study conception and data interpretation. MAK supervised the manufacturing and quality control of the ABCB5$^+$ MSCs, planned and supervised the *in vitro* experiments and preclinical trials and was substantially involved in data interpretation and conception and reviewing of the manuscript. All authors read and approved the final manuscript.

Acknowledgements

The authors thankfully acknowledge Charles River Laboratories France (Saint-Germain-Nuelles, France) and Preclinics GmbH (Potsdam, Germany) for performing the animal experiments, AnaPath GmbH (Oberbuchsiten, Switzerland) for histopathological examinations, and FGK Clinical Research GmbH (Munich, Germany) for expert support in project managing, monitoring, and data analysis of the clinical trial.

Author's information

Current affiliation:
GD: Clinic of Dermatology, Immunology and Allergology, Medical University Brandenburg "Theodor Fontane" Medical Center Dessau, Dessau, Germany

References

1. Armstrong DG, Boulton AJM, Bus SA. Diabetic Foot Ulcers and Their Recurrence. N Engl J Med. 2017;376:2367-75.
2. Jupiter DC, Thorud JC, Buckley CJ, Shibuya N. The impact of foot ulceration and amputation on mortality in diabetic patients. I: From ulceration to death, a systematic review. Int Wound J. 2016;13:892-903.
3. Xiang J, Wang S, He Y, Xu L, Zhang S, Tang Z. Reasonable Glycemic Control Would Help Wound Healing During the Treatment of Diabetic Foot Ulcers. Diabetes Ther. 2019;10:95-105.
4. Walsh JW, Hoffstad OJ, Sullivan MO, Margolis DJ. Association of diabetic foot ulcer and death in a population-based cohort from the United Kingdom. Diabet Med. 2016;33:1493-8.

5. Young MJ, McCardle JE, Randall LE, Barclay JI. Improved survival of diabetic foot ulcer patients 1995-2008: possible impact of aggressive cardiovascular risk management. Diabetes Care. 2008;31:2143-7.
6. Chammas NK, Hill RL, Edmonds ME. Increased Mortality in Diabetic Foot Ulcer Patients: The Significance of Ulcer Type. J Diabetes Res. 2016;2016:2879809.
7. Dietrich I, Braga GA, de Melo FG, da Costa Silva Silva ACC. The Diabetic Foot as a Proxy for Cardiovascular Events and Mortality Review. Curr Atheroscler Rep. 2017;19:44.
8. Martins-Mendes D, Monteiro-Soares M, Boyko EJ, Ribeiro M, Barata P, Lima J, et al. The independent contribution of diabetic foot ulcer on lower extremity amputation and mortality risk. J Diabetes Complications. 2014;28:632-8.
9. Brennan MB, Hess TM, Bartle B, Cooper JM, Kang J, Huang ES, et al. Diabetic foot ulcer severity predicts mortality among veterans with type 2 diabetes. J Diabetes Complications. 2017;31:556-61.
10. Prompers L, Huijberts M, Apelqvist J, Jude E, Piaggesi A, Bakker K, et al. High prevalence of ischaemia, infection and serious comorbidity in patients with diabetic foot disease in Europe. Baseline results from the Eurodiale study. Diabetologia. 2007;50:18-25.
11. Richard JL, Lavigne JP, Got I, Hartemann A, Malgrange D, Tsirtsikolou D, et al. Management of patients hospitalized for diabetic foot infection: results of the French OPIDIA study. Diabetes Metab. 2011;37:208-15.
12. Mutluoglu M, Sivrioglu AK, Eroglu M, Uzun G, Turhan V, Ay H, et al. The implications of the presence of osteomyelitis on outcomes of infected diabetic foot wounds. Scand J Infect Dis. 2013;45:497-503.
13. Ugwu E, Adeleye O, Gezawa I, Okpe I, Enamino M, Ezeani I. Predictors of lower extremity amputation in patients with diabetic foot ulcer: findings from MEDFUN, a multi-center observational study. J Foot Ankle Res. 2019;12:34.
14. Seth A, Attri AK, Kataria H, Kochhar S, Seth SA, Gautam N. Clinical Profile and Outcome in Patients of Diabetic Foot Infection. Int J Appl Basic Med Res. 2019;9:14-9.
15. Armstrong DG, Swerdlow MA, Armstrong AA, Conte MS, Padula WV, Bus SA. Five year mortality and direct costs of care for people with diabetic foot complications are comparable to cancer. J Foot Ankle Res. 2020;13:16.
16. Ince P, Game FL, Jeffcoate WJ. Rate of healing of neuropathic ulcers of the foot in diabetes and its relationship to ulcer duration and ulcer area. Diabetes Care. 2007;30:660-3.
17. Zelen CM, Orgill DP, Serena T, Galiano R, Carter MJ, DiDomenico LA, et al. A prospective, randomised, controlled, multicentre clinical trial examining healing rates, safety and cost to closure of an acellular reticular allogenic human dermis versus standard of care in the treatment of chronic diabetic foot ulcers. Int Wound J. 2017;14:307-15.
18. Ha Van G, Amouyal C, Bourron O, Aubert C, Carlier A, Mosbah H, et al. Diabetic foot ulcer management in a multidisciplinary foot centre: one-year healing, amputation and mortality rate. J Wound Care. 2020;29:464-71.

19. Lavery LA, Davis KE, Berriman SJ, Braun L, Nichols A, Kim PJ, et al. WHS guidelines update: Diabetic foot ulcer treatment guidelines. Wound Repair Regen. 2016;24:112-26.
20. Hingorani A, LaMuraglia GM, Henke P, Meissner MH, Loretz L, Zinszer KM, et al. The management of diabetic foot: A clinical practice guideline by the Society for Vascular Surgery in collaboration with the American Podiatric Medical Association and the Society for Vascular Medicine. J Vasc Surg. 2016;63:3s-21s.
21. Ousey K, Chadwick P, Jawien A, Tariq G, Nair HKR, Lázaro-Martínez JL, et al. Identifying and treating foot ulcers in patients with diabetes: saving feet, legs and lives. J Wound Care. 2018;27:S1-s52.
22. Schaper NC, van Netten JJ, Apelqvist J, Bus SA, Hinchliffe RJ, Lipsky BA. Practical Guidelines on the prevention and management of diabetic foot disease (IWGDF 2019 update). Diabetes Metab Res Rev. 2020;36 Suppl 1:e3266.
23. Vas P, Rayman G, Dhatariya K, Driver V, Hartemann A, Londahl M, et al. Effectiveness of interventions to enhance healing of chronic foot ulcers in diabetes: a systematic review. Diabetes Metab Res Rev. 2020;36 Suppl 1:e3284.
24. Okonkwo UA, DiPietro LA. Diabetes and Wound Angiogenesis. Int J Mol Sci. 2017;18.
25. Burgess JL, Wyant WA, Abdo Abujamra B, Kirsner RS, Jozic I. Diabetic Wound-Healing Science. Medicina (Kaunas). 2021;57.
26. Rehak L, Giurato L, Meloni M, Panunzi A, Manti GM, Uccioli L. The Immune-Centric Revolution in the Diabetic Foot: Monocytes and Lymphocytes Role in Wound Healing and Tissue Regeneration-A Narrative Review. J Clin Med. 2022;11.
27. Catrina SB, Zheng X. Disturbed hypoxic responses as a pathogenic mechanism of diabetic foot ulcers. Diabetes Metab Res Rev. 2016;32 Suppl 1:179-85.
28. Wetzler C, Kämpfer H, Stallmeyer B, Pfeilschifter J, Frank S. Large and sustained induction of chemokines during impaired wound healing in the genetically diabetic mouse: prolonged persistence of neutrophils and macrophages during the late phase of repair. J Invest Dermatol. 2000;115:245-53.
29. Mirza R, Koh TJ. Dysregulation of monocyte/macrophage phenotype in wounds of diabetic mice. Cytokine. 2011;56:256-64.
30. Mirza RE, Fang MM, Ennis WJ, Koh TJ. Blocking interleukin-1β induces a healing-associated wound macrophage phenotype and improves healing in type 2 diabetes. Diabetes. 2013;62:2579-87.
31. Mirza RE, Fang MM, Weinheimer-Haus EM, Ennis WJ, Koh TJ. Sustained inflammasome activity in macrophages impairs wound healing in type 2 diabetic humans and mice. Diabetes. 2014;63:1103-14.
32. Bannon P, Wood S, Restivo T, Campbell L, Hardman MJ, Mace KA. Diabetes induces stable intrinsic changes to myeloid cells that contribute to chronic inflammation during wound healing in mice. Dis Model Mech. 2013;6:1434-47.
33. Aitcheson SM, Frentiu FD, Hurn SE, Edwards K, Murray RZ. Skin Wound Healing: Normal Macrophage Function and Macrophage Dysfunction in Diabetic Wounds. Molecules. 2021;26.

34. Mace KA, Yu DH, Paydar KZ, Boudreau N, Young DM. Sustained expression of Hif-1alpha in the diabetic environment promotes angiogenesis and cutaneous wound repair. Wound Repair Regen. 2007;15:636-45.
35. Botusan IR, Sunkari VG, Savu O, Catrina AI, Grünler J, Lindberg S, et al. Stabilization of HIF-1alpha is critical to improve wound healing in diabetic mice. Proc Natl Acad Sci U S A. 2008;105:19426-31.
36. Catrina SB, Okamoto K, Pereira T, Brismar K, Poellinger L. Hyperglycemia regulates hypoxia-inducible factor-1alpha protein stability and function. Diabetes. 2004;53:3226-32.
37. Thangarajah H, Yao D, Chang EI, Shi Y, Jazayeri L, Vial IN, et al. The molecular basis for impaired hypoxia-induced VEGF expression in diabetic tissues. Proc Natl Acad Sci U S A. 2009;106:13505-10.
38. Zubair M, Ahmad J. Role of growth factors and cytokines in diabetic foot ulcer healing: A detailed review. Rev Endocr Metab Disord. 2019;20:207-17.
39. Singh AK, Gudehithlu KP, Patri S, Litbarg NO, Sethupathi P, Arruda JA, et al. Impaired integration of endothelial progenitor cells in capillaries of diabetic wounds is reversible with vascular endothelial growth factor infusion. Transl Res. 2007;149:282-91.
40. Okonkwo UA, Chen L, Ma D, Haywood VA, Barakat M, Urao N, et al. Compromised angiogenesis and vascular Integrity in impaired diabetic wound healing. PLoS One. 2020;15:e0231962.
41. Lopes L, Setia O, Aurshina A, Liu S, Hu H, Isaji T, et al. Stem cell therapy for diabetic foot ulcers: a review of preclinical and clinical research. Stem Cell Res Ther. 2018;9:188.
42. Huang YZ, Gou M, Da LC, Zhang WQ, Xie HQ. Mesenchymal Stem Cells for Chronic Wound Healing: Current Status of Preclinical and Clinical Studies. Tissue Eng Part B Rev. 2020.
43. Cho H, Blatchley MR, Duh EJ, Gerecht S. Acellular and cellular approaches to improve diabetic wound healing. Adv Drug Deliv Rev. 2019;146:267-88.
44. Jiang D, Scharffetter-Kochanek K. Mesenchymal Stem Cells Adaptively Respond to Environmental Cues Thereby Improving Granulation Tissue Formation and Wound Healing. Front Cell Dev Biol. 2020;8:697.
45. Singh K, Maity P, Koroma AK, Basu A, Pandey RK, Beken SV, et al. Angiogenin Released from ABCB5(+) Stromal Precursors Improves Healing of Diabetic Wounds by Promoting Angiogenesis. J Invest Dermatol 2021; doi:10.1016/j.jid.2021.10.026.
46. Schatton T, Yang J, Kleffel S, Uehara M, Barthel SR, Schlapbach C, et al. ABCB5 Identifies Immunoregulatory Dermal Cells. Cell Rep. 2015;12:1564-74.
47. Jiang D, Muschhammer J, Qi Y, Kugler A, de Vries JC, Saffarzadeh M, et al. Suppression of Neutrophil-Mediated Tissue Damage - A Novel Skill of Mesenchymal Stem Cells. Stem Cells. 2016;34:2393-406.
48. Vander Beken S, de Vries JC, Meier-Schiesser B, Meyer P, Jiang D, Sindrilaru A, et al. Newly Defined ATP-Binding Cassette Subfamily B Member 5 Positive Dermal Mesenchymal Stem Cells Promote Healing of Chronic Iron-Overload Wounds via Secretion of Interleukin-1 Receptor Antagonist. Stem Cells. 2019;37:1057-74.

49. Kerstan A, Niebergall-Roth E, Esterlechner J, Schröder HM, Gasser M, Waaga-Gasser AM, et al. Ex vivo-expanded highly pure ABCB5(+) mesenchymal stromal cells as Good Manufacturing Practice-compliant autologous advanced therapy medicinal product for clinical use: process validation and first in-human data. Cytotherapy. 2021;23:165-75.
50. Kerstan A, Dieter K, Niebergall-Roth E, Dachtler A-K, Kraft K, Stücker M, et al. Allogeneic ABCB5(+) mesenchymal stem cells for treatment-refractory chronic venous ulcers: a phase I/IIa clinical trial. JID Innovations. 2022;2:100067.
51. Ballikaya S, Sadeghi S, Niebergall-Roth E, Nimtz L, Frindert J, Norrick A, et al. Process data of allogeneic ex vivo-expanded ABCB5+ mesenchymal stromal cells for human use: off-the-shelf GMP-manufactured donor-independent ATMP. Stem Cell Research & Therapy. 2020;11:482.
52. Tappenbeck N, Schröder HM, Niebergall-Roth E, Hassinger F, Dehio U, Dieter K, et al. In vivo safety profile and biodistribution of GMP-manufactured human skin-derived ABCB5-positive mesenchymal stromal cells for use in clinical trials. Cytotherapy. 2019;21:546-60.
53. Frank NY, Pendse SS, Lapchak PH, Margaryan A, Shlain D, Doeing C, et al. Regulation of progenitor cell fusion by ABCB5 P-glycoprotein, a novel human ATP-binding cassette transporter. J Biol Chem. 2003;278:47156-65.
54. National Institute for Health and Care Excellence. Diabetic foot problems: prevention and management – NICE guideline. 2015. https://www.nice.org.uk/guidance/ng19/resources/diabetic-foot-problems-prevention-and-management-pdf-1837279828933. Accessed 20 Dec 2021.
55. The International Working Group on the Diabetic Foot (IWGDF). IWGDF Practical guidelines on the prevention and management of diabetic foot disease. 2019. https://iwgdfguidelines.org/wp-content/uploads/2019/05/01-IWGDF-practical-guidelines-2019.pdf. Accessed 20 Dec 2021.
56. Wendelken ME, Berg WT, Lichtenstein P, Markowitz L, Comfort C, Alvarez OM. Wounds measured from digital photographs using photodigital planimetry software: validation and rater reliability. Wounds. 2011;23:267-75.
57. Romanelli M, Vowden K, Weir D. Exudate management made easy. 2010. https://www.woundsinternational.com/resources/details/exudate-management-made-easy. Accessed 20 Dec 2021.
58. Perrault DP, Bramos A, Xu X, Shi S, Wong AK. Local Administration of Interleukin-1 Receptor Antagonist Improves Diabetic Wound Healing. Ann Plast Surg. 2018;80:S317-s21.
59. Tan JL, Lash B, Karami R, Nayer B, Lu Y-Z, Piotto C, et al. Restoration of the healing microenvironment in diabetic wounds with matrix-binding IL-1 receptor antagonist. Communications Biology. 2021;4:422.
60. Duscher D, Januszyk M, Maan ZN, Whittam AJ, Hu MS, Walmsley GG, et al. Comparison of the Hydroxylase Inhibitor Dimethyloxalylglycine and the Iron Chelator Deferoxamine in Diabetic and Aged Wound Healing. Plast Reconstr Surg. 2017;139:695e-706e.
61. Li G, Ko C-N, Li D, Yang C, Wang W, Yang G-J, et al. A small molecule HIF-1α stabilizer that accelerates diabetic wound healing. Nature Communications. 2021;12:3363.

62. Galiano RD, Tepper OM, Pelo CR, Bhatt KA, Callaghan M, Bastidas N, et al. Topical vascular endothelial growth factor accelerates diabetic wound healing through increased angiogenesis and by mobilizing and recruiting bone marrow-derived cells. Am J Pathol. 2004;164:1935-47.
63. Akash MS, Rehman K, Chen S. IL-1Ra and its delivery strategies: inserting the association in perspective. Pharm Res. 2013;30:2951-66.
64. Nurkesh A, Jaguparov A, Jimi S, Saparov A. Recent Advances in the Controlled Release of Growth Factors and Cytokines for Improving Cutaneous Wound Healing. Front Cell Dev Biol. 2020;8:638.
65. Chamboredon S, Ciais D, Desroches-Castan A, Savi P, Bono F, Feige JJ, et al. Hypoxia-inducible factor-1alpha mRNA: a new target for destabilization by tristetraprolin in endothelial cells. Mol Biol Cell. 2011;22:3366-78.
66. Hofmann NA, Ortner A, Jacamo RO, Reinisch A, Schallmoser K, Rohban R, et al. Oxygen sensing mesenchymal progenitors promote neo-vasculogenesis in a humanized mouse model in vivo. PLoS One. 2012;7:e44468.
67. Riedl J, Pickett-Leonard M, Eide C, Kluth MA, Ganss C, Frank NY, et al. ABCB5+ dermal mesenchymal stromal cells with favorable skin homing and local immunomodulation for recessive dystrophic epidermolysis bullosa treatment. Stem Cells. 2021;39:897-903.
68. Atkin L, Bućko Z, Conde Montero E, Cutting K, Moffatt C, Probst A, et al. Implementing TIMERS: the race against hard-to-heal wounds. J Wound Care. 2019;23:S1-s50.
69. Caplan AI. Cell-Based Therapies: The Nonresponder. Stem Cells Transl Med. 2018;7:762-6.
70. Levy O, Kuai R, Siren EMJ, Bhere D, Milton Y, Nissar N, et al. Shattering barriers toward clinically meaningful MSC therapies. Sci Adv. 2020;6:eaba6884.
71. Margolis DJ, Kantor J, Santanna J, Strom BL, Berlin JA. Risk factors for delayed healing of neuropathic diabetic foot ulcers: a pooled analysis. Arch Dermatol. 2000;136:1531-5.
72. Margolis DJ, Allen-Taylor L, Hoffstad O, Berlin JA. Diabetic neuropathic foot ulcers: the association of wound size, wound duration, and wound grade on healing. Diabetes Care. 2002;25:1835-9.
73. Margolis DJ, Allen-Taylor L, Hoffstad O, Berlin JA. Diabetic neuropathic foot ulcers: predicting which ones will not heal. Am J Med. 2003;115:627-31.
74. Prompers L, Schaper N, Apelqvist J, Edmonds M, Jude E, Mauricio D, et al. Prediction of outcome in individuals with diabetic foot ulcers: focus on the differences between individuals with and without peripheral arterial disease. The EURODIALE Study. Diabetologia. 2008;51:747-55.
75. Roth-Albin I, Mai SHC, Ahmed Z, Cheng J, Choong K, Mayer PV. Outcomes Following Advanced Wound Care for Diabetic Foot Ulcers: A Canadian Study. Can J Diabetes. 2017;41:26-32.
76. Fife CE, Horn SD, Smout RJ, Barrett RS, Thomson B. A Predictive Model for Diabetic Foot Ulcer Outcome: The Wound Healing Index. Adv Wound Care (New Rochelle). 2016;5:279-87.
77. Tong T, Yang C, Tian W, Liu Z, Liu B, Cheng J, et al. Phenotypes and outcomes in middle-aged patients with diabetic foot ulcers: a retrospective cohort study. J Foot Ankle Res. 2020;13:24.

78. Gazzaruso C, Gallotti P, Pujia A, Montalcini T, Giustina A, Coppola A. Predictors of healing, ulcer recurrence and persistence, amputation and mortality in type 2 diabetic patients with diabetic foot: a 10-year retrospective cohort study. Endocrine. 2021;71:59-68.
79. Wang A, Sun X, Wang W, Jiang K. A study of prognostic factors in Chinese patients with diabetic foot ulcers. Diabet Foot Ankle. 2014;5.
80. Dutra LMA, Melo MC, Moura MC, Leme LAP, De Carvalho MR, Mascarenhas AN, et al. Prognosis of the outcome of severe diabetic foot ulcers with multidisciplinary care. J Multidiscip Healthc. 2019;12:349-59.
81. Vella L, Gatt A, Formosa C. Does Baseline Hemoglobin A(1c) Level Predict Diabetic Foot Ulcer Outcome or Wound Healing Time? J Am Podiatr Med Assoc. 2017;107:272-9.
82. Theocharidis G, Baltzis D, Roustit M, Tellechea A, Dangwal S, Khetani RS, et al. Integrated Skin Transcriptomics and Serum Multiplex Assays Reveal Novel Mechanisms of Wound Healing in Diabetic Foot Ulcers. Diabetes. 2020;69:2157-69.
83. Margolis DJ, Hampton M, Hoffstad O, Mala DS, Mirza Z, Woltereck D, et al. NOS1AP genetic variation is associated with impaired healing of diabetic foot ulcers and diminished response to healing of circulating stem/progenitor cells. Wound Repair Regen. 2017;25:733-6.
84. Mir KA, Pugazhendhi S, Paul MJ, Nair A, Ramakrishna BS. Heat-shock protein 70 gene polymorphism is associated with the severity of diabetic foot ulcer and the outcome of surgical treatment. Br J Surg. 2009;96:1205-9.
85. Davis FM, Kimball A, Boniakowski A, Gallagher K. Dysfunctional Wound Healing in Diabetic Foot Ulcers: New Crossroads. Curr Diab Rep. 2018;18:2.
86. U.S. Department of Health and Human Services, Food and Drug Administration. Guidance for Industry: Chronic Cutaneous Ulcer and Burn Wounds – Developing Products for Treatment. 2006. https://www.fda.gov/media/71278/download. Accessed 20 Dec 2021.
87. European Parliament and Council of the European Union. Directive 2010/63/EU of the European Parliament and of the Council of 22 September 2010 on the protection of animals used for scientific purposes. Official Journal of the European Union. 2010;L276:33-79.

Figures

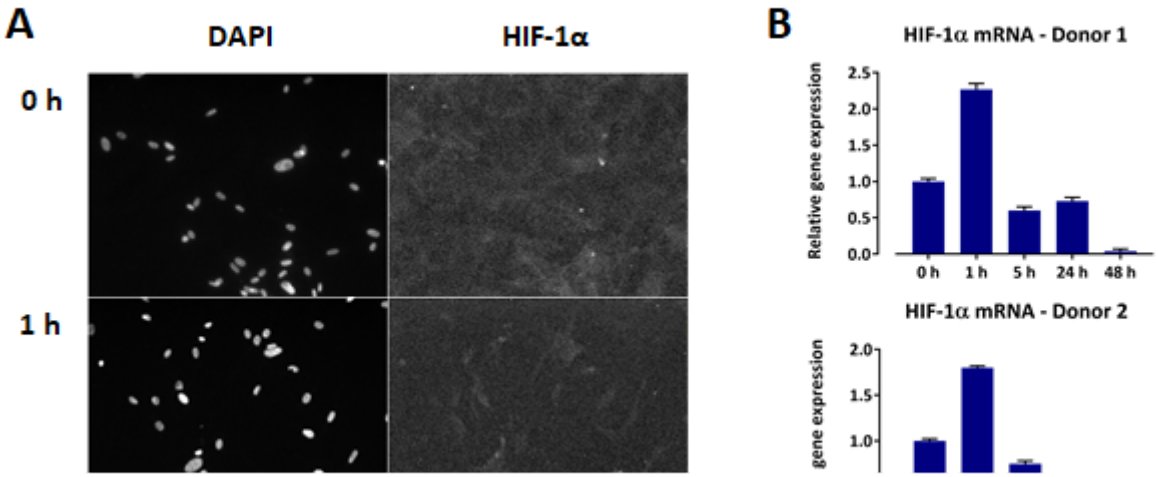

Figure 1

HIF-1α and VEGF expression by ABCB5$^+$ MSCs during 48 h hypoxic culture. **A** Representative immunofluorescence staining of ABCB5$^+$ MSCs revealing nuclear translocation of HIF-1α. Nuclei were counterstained with DAPI. **B** HIF-1α mRNA expression by ABCB5$^+$ MSCs from two donors, shown as fold expression from baseline (normoxic conditions, 0 h). Data are means + SD of three replicates. **C** VEGF mRNA expression by ABCB5$^+$ MSCs, shown as fold expression from baseline (normoxic conditions, 0 h). Data are means + SD of three donors. **D** VEGF protein secretion by ABCB5$^+$ MSCS, measured as VEGF protein concentration in culture supernatant. Data are means + SD of three replicates from a representative donor.

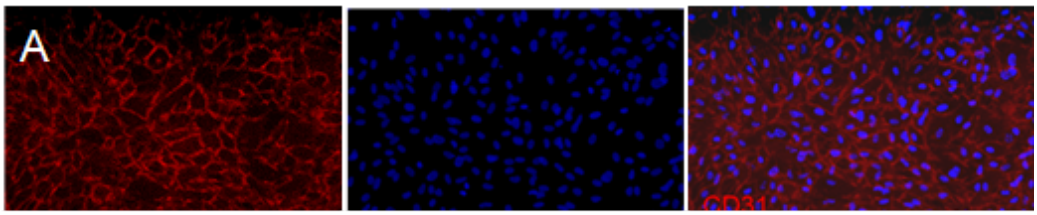

Figure 2

Endothelial trans-differentiation of ABCB5$^+$ MSCs. **A** Co-stimulation for 96 h with 200 ng/ml VEGF, 1000 ng/ml FGF-2 and 1000 ng/ml PDGF-BB elicited angiogenic trans-differentiation of ABCB5$^+$ MSCs as revealed by CD31-positive (red) staining. **B** ABCB5$^+$ MSCs cultured without growth factor supplementation served as negative control. **C** HUVECs served as positive control. **D–F** Proliferative

activity of ABCB5^{+} MSCs stimulated to undergo endothelial trans-differentiation. **D** ABCB5^{+} MSCs were stimulated for 96 h with 200 ng/ml VEGF, 1000 ng/ml FGF-2 and 1000 ng/ml PDGF-BB. Proliferative activity was assessed by Ki-67 staining (red). **E** ABCB5^{+} MSCs cultured without growth factor supplementation served as negative control. **F** HUVECs served as positive control. Nuclei were counterstained with DAPI (blue). Representative images of three independent experiments.

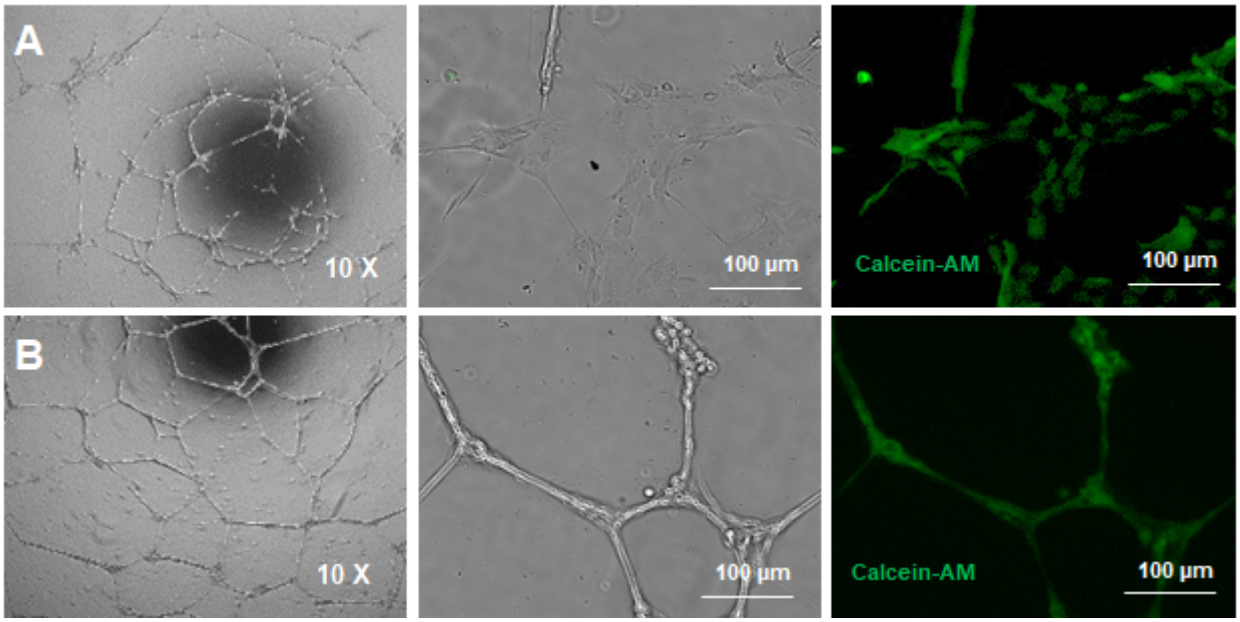

Figure 3

Tube formation assays. **A** Human ABCB5^{+} MSCs and **B** HUVECs were cultured for 18–20 h on Geltrex^{TM} matrix. Calcein staining (green) demonstrates viability (*i.e.,* metabolic activity) of tubular structure-forming cells.

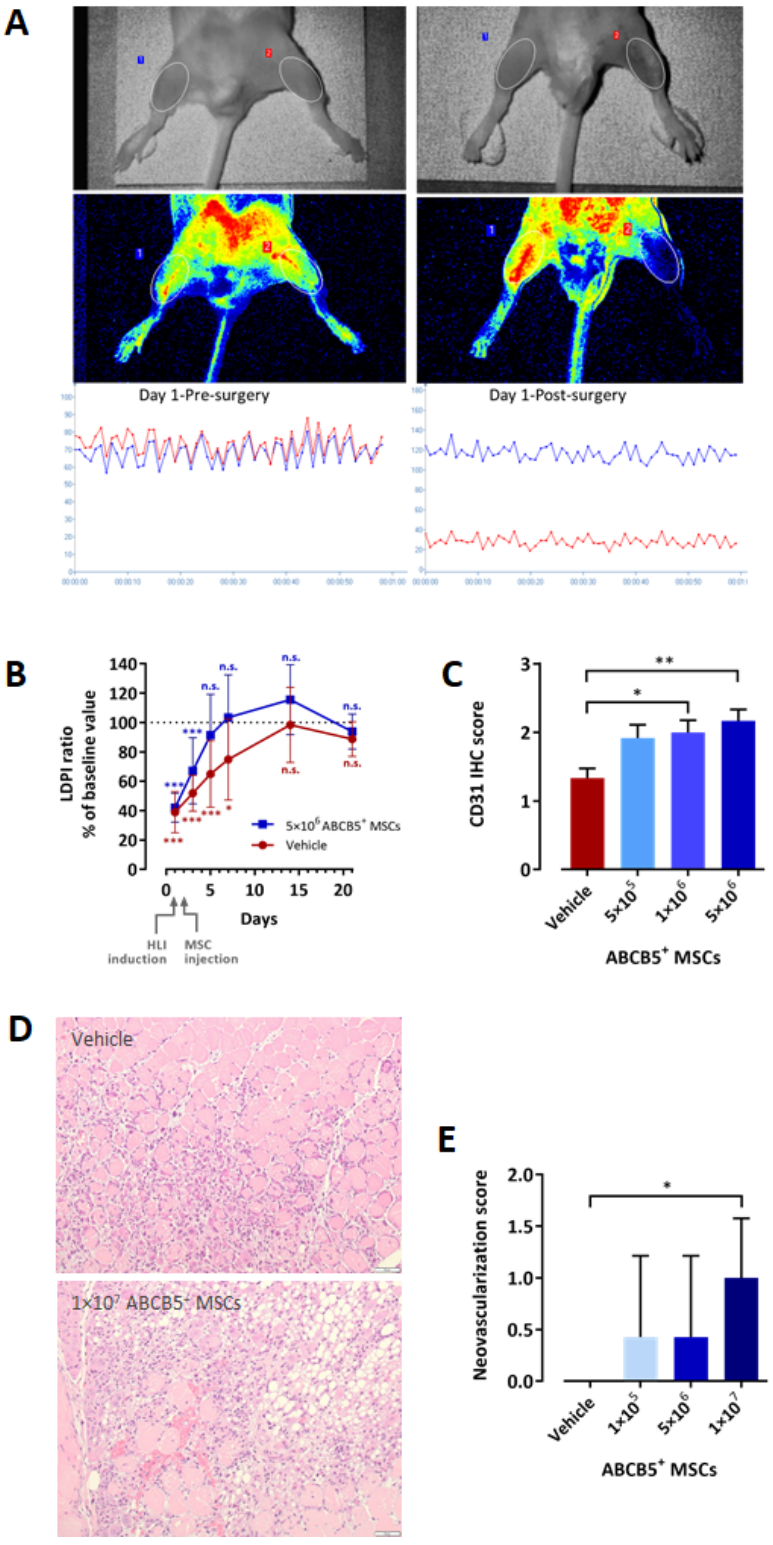

Figure 4

Blood flow recovery and neovascularization following surgically induced HLI in OF1 mice.
A Representative LDPI acquisition before and immediately after HLI induction. Scanned areas are marked by ellipses. Measurements are expressed as perfusion units, with the warmest color (intense red) representing 200 perfusion units. Graphs show mean perfusion unit during 1 min in the non-ischemic (blue) and ischemic (red) thigh. **B** LPDI ratio between the ischemic and the non-ischemic limb, expressed

as percentage of the baseline (pre-surgery) value, in mice treated with 5×10^6 ABCB5$^+$ MSCs or vehicle. Means with SD of n=10 (day 1), n=9 (day 3), n=8 (day 5; days 7–21 MSC) and n=7 (days 7–21 vehicle) animals. **C** Immunohistochemical evaluation of CD31 expression in the ischemic thigh muscles at 6 days after HLI induction in mice treated with ABCB5$^+$ MSCs or vehicle injected into the ischemic limb 24 h after surgery. Expression was semi-quantitatively rated as 0 = none, 1 = minimal, 2 = slight, and 3 = moderate. Means with SD of n=12 animals. **D-E** Histopathological evaluation of neovascularization in the ischemic gastrocnemius muscles at 6 days after HLI induction in mice treated with ABCB5$^+$ MSCs or vehicle injected into the ischemic limb 24 h after surgery. **D** Representative H&E sections from a vehicle- and an MSC-treated mouse, showing inflammatory and degenerative lesions in both mice and increased neovascularization in the MSC-treated mouse. Magnification ×20; scale bars: 50 μm. **E** Semi-quantitative assessment of neovascularization with 0 = none, 1 = 1–3 focal buds, 2 = groups of 4–7 capillaries with supporting fibroblastic structures, 3 = broad band and 4 = extensive band of capillaries with supporting fibroblastic structures. Means with SD of n=7 (MSC-treated) and n=6 (vehicle) animals. *p<0.05, **p<0.01, ***p<0.001 vs. baseline (B) or vehicle (C, E); one-way ANOVA with Dunnett's post-hoc test.

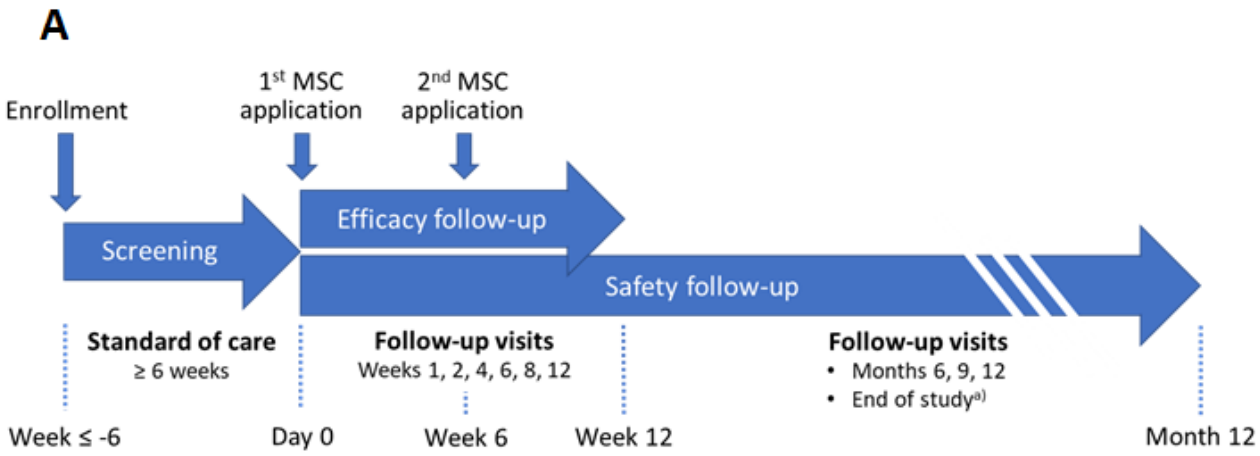

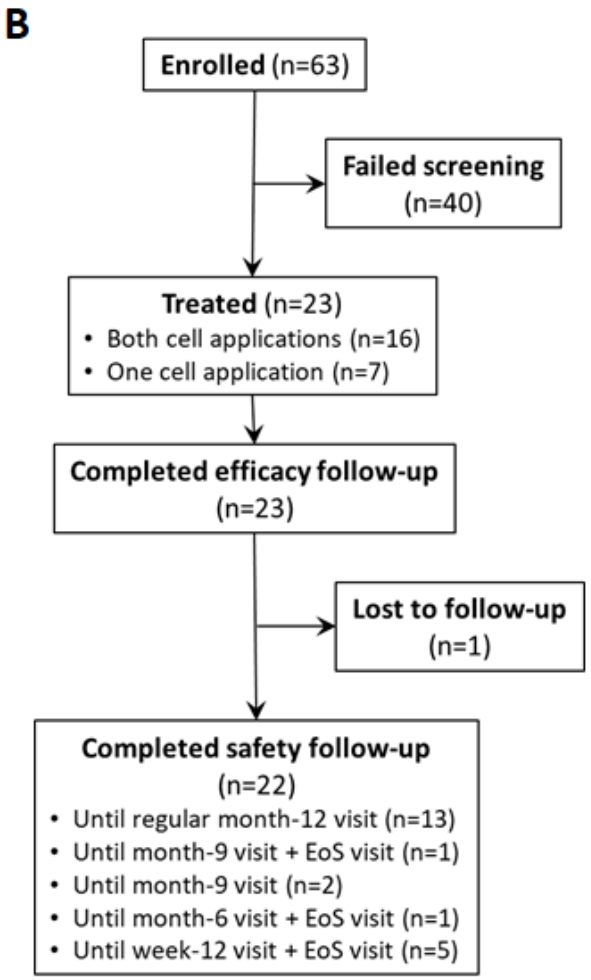

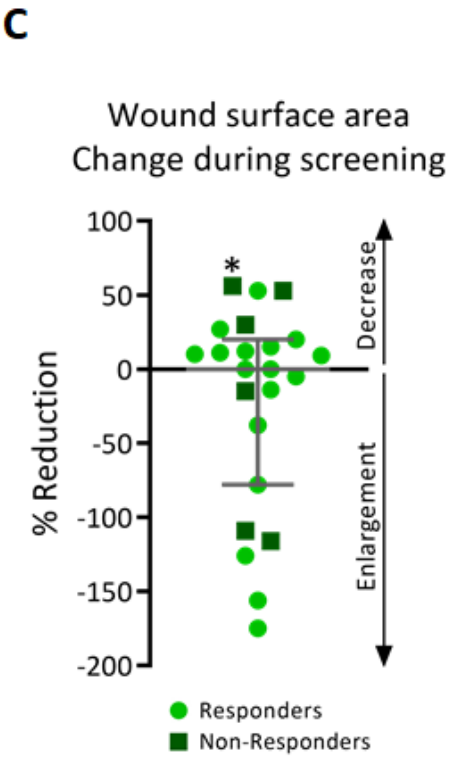

Figure 5

Trial design, study patients and wound surface area during screening. **A** Schematic representation of the trial design. [a]Only patients who did not reach month-12 visit before 30 June 2020 and were not scheduled for a planned safety follow-up visit in June 2020 were subjected to an end-of-study visit. **B** Study patient flow chart. EoS visit, end-of-study visit [see (a)]. **C** Percent reduction of wound surface area during a

≥6-week screening period (median 49 days, range 42-68 days; except for one outlier, whose screening period lasted 118 days, denoted by an asterisk). Error bar represents median and interquartile range.

Figure 6

Wound healing progress during the treatment and efficacy follow-up period. Shown are three representative patients in the subgroup of responders. All patients had consented to publication of the photographs.

Figure 7

Wound surface area reduction in DFU patients treated with ABCB5$^+$ MSCs. **A-B** Percent wound surface area reduction from baseline during the treatment and efficacy follow-up period in the full analysis set (**A**) and per-protocol set (**B**). Patients who presented with wound surface area reductions of at least 30% from baseline (indicated by light green dashed lines) at week 12 were considered responders. Error bars indicate median and interquartile range; *p* values (two-sided Wilcoxon signed rank test) indicate statistical significance of changes from baseline. **C** Tukey's boxplots of the primary efficacy outcome parameter, % wound surface area reduction from baseline at week 12, in the full analysis set (FAS, N=23), per-protocol set (PP, N=20) and responders (*i.e.* patients who presented with at least 30% wound surface area at week 12; N=17). **D-E** Kaplan–Meier plots for the time to full wound closure (**D**) and first 30% surface area reduction (**E**) in the FAS, PP and responders. Patients without event were censored at the date of the last available wound surface area assessment (indicated by small vertical ticks). Vertical dashed lines indicate median time to event (not reached for full wound closure).

Figure 8

Assessment of potential influences of baseline patient characteristic, baseline wound size and wound surface area reduction during the screening period on response to treatment. Baseline patient characteristics and baseline wound surface area in all treated patients, responders and non-responders. **A– B** Comparisons of baseline patient characteristics (**A**) and of wound surface area reduction during screening and of wound surface area at baseline (**B**) between all treated patients, responders and non-responders. Depicted are Tukey's boxplots (except for gender ratio); n=23 (all patients; ankle-brachial index: n=22), n=17 (responders; ankle-brachial index: n=16), n=6 (non-responders). Kruskal-Wallis tests followed by Dunn's multiple comparisons revealed no statistically significant differences between groups ($p>0.999$ for all comparisons except for ankle-brachial index responders *vs.* non-responders: $p=0.697$). **C** Spearman's rank correlation analysis between wound surface area reduction during screening and

wound surface area reduction from baseline at week 12. *Asterisk denotes a patient whose screening period lasted 118 days, as compared to 42–68 days (median 49 days) for the other patients.

Supplementary Files

This is a list of supplementary files associated with this preprint. Click to download.

- Kerstanetal.Additionalfile1.docx
- Kerstanetal.Additionalfile2.docx